SPARSITY-PROMOTING METHODS FOR ISOLATING DOMINANT LINEAR AMPLIFICATION MECHANISMS IN TURBULENT FLOWS

Scott T. M. Dawson
MMAE Department
Illinois Institute of Technology
Chicago, Illinois, 60616 USA
scott.dawson@iit.edu

Jaime Prado Zayas
MMAE Department
Illinois Institute of Technology
Chicago, Illinois, 60616 USA
jpradozayas@hawk.iit.edu

Barbara Lopez-Doriga
MMAE Department
Illinois Institute of Technology
Chicago, Illinois, 60616 USA
blopezdorigacostales@hawk.iit.edu

ABSTRACT
This work proposes a method to identify and isolate the physical mechanisms that are responsible for linear energy amplification in turbulent flows. This is achieved by applying a sparsity-promoting methodology to the resolvent form of the governing equations, solving an optimization problem that balances retaining the amplification properties of the original operator with minimizing the number of terms retained in the simplified sparse model. This results in simplified operators that often have very similar pseudospectral properties as the original equations. The method is demonstrated on both incompressible and compressible wall-bounded parallel shear flows, where the results obtained from the proposed method are shown to be consistent with known mechanisms and simplifying assumptions, such as the lift-up mechanism, and (for the compressible case) Morkovin's hypothesis and the strong Reynolds analogy. This provides a framework for the application of this method to problems for which knowledge of pertinent amplification mechanisms is less established.

INTRODUCTION
Despite the fact that turbulence exhibits highly nonlinear dynamics, there is strong evidence that linear mechanisms play a key role in both the formation of coherent structures within, and the overall statistics of, such flows. This is particularly true for shear-driven turbulence, where spatial gradients of the mean velocity field and the non-normality of the linearized equations can drive very large linear amplification (Trefethen *et al.*, 1993; Schmid & Henningson, 2012; Hwang & Cossu, 2010). Indeed, several recent works (Abreu *et al.*, 2020; Tissot *et al.*, 2021; Nogueira *et al.*, 2021; Pickering *et al.*, 2021; Symon *et al.*, 2023) have demonstrated agreement between coherent structure prediction via resolvent analysis of the mean-linearized equations (McKeon & Sharma, 2010), and the highest-energy structures identified directly from data via spectral spectral proper orthogonal decomposition (Towne *et al.*, 2018).

In configurations that have been comprehensively studied, there is broad understanding of both the characteristics of coherent structures that form in turbulent flows, and the mechanisms that lead to their formulation. In canonical wall-bounded turbulent flows, the Orr (Orr, 1907) and lift-up (Landahl, 1975) mechanisms play a key role in the generation and evolution of features such as near-wall streaks (Kline *et al.*, 1967), and large- and very-large-scale motions (Zhou *et al.*, 1999; Hutchins & Marusic, 2007). In particular, the mechanisms giving rise to such structures can be understood through the action of a small number of terms within the governing equations. The development of a similar level of understanding for a broader class of more complex, non-canonical geometries can be accelerated through methods that can automatically identify the terms within the governing equations that are primarily responsible for the dominant coherent features observed in such systems.

The present work develops a method to automatically extract such minimal-physics mechanisms from the governing equations. This is achieved through utilizing ideas from compressive sensing (Candès *et al.*, 2006), which allows for such problems to be solved with convex methods, by formulating optimization problems involving the L_1 norm. Such sparsity-promoting methods have been used for a range of data-driven problems in fluid mechanics, such as the identification of sparse reduced-order models (Loiseau & Brunton, 2018; Rubini *et al.*, 2020), and in using data to identify active terms in the governing equations (Callaham *et al.*, 2021). By contrast, the present approach is largely data-free, applying sparsity-promotion directly upon the governing equations. This work focuses on analysis of the resolvent form of the mean-linearized Navier–Stokes equations. Sparsity-promotion has previously been applied in such analyses for the purposes of identifying spatially (Foures *et al.*, 2013; Skene *et al.*, 2022) or spatio-temporally localized (Lopez-Doriga *et al.*, 2024) structures. Here, rather than seeking sparsity in the structures corresponding to linear amplification mechanisms, we instead seek to sparsify the underlying linear operator, in order to identify the components of the operator that are primarily responsible for the leading linear energy amplification mechanisms identified through resolvent analysis.

METHODOLOGY
Resolvent Analysis
We describe the resolvent methodology in the context of incompressible parallel shear flow, formulated in wall-normal velocity (v) and vorticity (η) coordinates. After performing Fourier transforms in the streamwise (x) and spanwise (z) directions and in time (t), the Navier–Stokes equations may be

written in resolvent form as (Rosenberg & McKeon, 2019)

$$\begin{pmatrix} \hat{v} \\ \hat{\eta} \end{pmatrix} = \underbrace{\begin{pmatrix} \mathscr{H}_{OS} & 0 \\ ik_z \mathscr{H}_{SQ} U_y \mathscr{H}_{OS} & \mathscr{H}_{SQ} \end{pmatrix}}_{\mathscr{H}} \begin{pmatrix} \hat{f}_v \\ \hat{f}_\eta \end{pmatrix} \tag{1}$$

$$\mathscr{H}_{OS} = \left(-i\omega + \Delta^{-1} \left[ik_x U \Delta - ik_x U_{yy} - \frac{1}{Re} \Delta^2 \right] \right)^{-1} \tag{2}$$

$$\mathscr{H}_{SQ} = \left(-i\omega + ik_x U - \frac{1}{Re} \Delta \right)^{-1} \tag{3}$$

where $\mathscr{H}$ is the resolvent operator, expressed in terms of the resolvent Orr-Sommerfeld ($\mathscr{H}_{OS}$) and Squire ($\mathscr{H}_{SQ}$) components. Here ω is a the temporal frequency, k_x and k_z are streamwise and spanwise wavenumbers, Δ is the Laplacian operator, and U, U_y and U_{yy} are the mean streamwise velocity and its first and second derivatives in the wall-normal (y) direction. The $\hat{}$ notation indicates that we are working with Fourier-transformed variables in the x, z, and t dimensions. The incompressible turbulent mean profiles are obtained by assuming an eddy viscosity model. The quantities $\hat{f}_v$ and $\hat{f}_\eta$ denote forcing terms in the v and η components respectively, which here can incorporate the effect of unmodeled nonlinear terms. To explore the broader applicability of our proposed method, we will also consider here equivalent formulation for the compressible Navier–Stokes equations, though for brevity we delay a description of the equivalent compressible operator to the results section.

The resolvent methodology proceeds by considering a singular value decomposition (SVD) of $\mathscr{H}$, with the leading left (ψ_i) and right (ϕ_1) singular vectors giving the resolvent response and forcing modes corresponding to largest amplification (quantified by the leading singular value, σ_1). This work will be focused on developing a method that can discover which blocks of the resolvent operator, as formulated in equation 1 for the incompressible case, are primarily responsible for the emergence of this leading mode, describing the dominant linear amplification mechanism. The numerical discretization of the resolvent operator is obtained using a Chebyshev collocation method.

Block-Sparsification of the Resolvent Operator

Here, we describe the methodology developed and applied in the present work. Before applying the method to the specific linearized operator described in the previous section, we first describe our approach in more general terms. Suppose we have a system of equations for the spatiotemporal dynamics of a quantity $\boldsymbol{u}(\boldsymbol{x},t)$ (e.g. a velocity field) that have the general form

$$\boldsymbol{f}\left(\boldsymbol{u}(\boldsymbol{x},t), \partial_t, \partial_{\boldsymbol{x}}\right) := \sum_j \boldsymbol{f}_j \left(\boldsymbol{u}(\boldsymbol{x},t), \partial_t, \partial_{\boldsymbol{x}}\right) = \mathbf{0} \tag{4}$$

Each of the terms $\boldsymbol{f}_j$ can include partial derivatives in time and space (∂_t and $\partial_{\boldsymbol{x}}$), so that equation 4 represents the partial differential equations describing the system of interest. The main idea underpinning the proposed methodology is that many physical phenomena can be understood without needing to consider all of the terms in this sum. Mathematically, first define generalized equations

$$\boldsymbol{f}_a\left(\boldsymbol{u}(\boldsymbol{x},t), \partial_t, \partial_{\boldsymbol{x}}; \mathbf{c}, \mathbf{d}\right) := \sum_j c_j \boldsymbol{f}_j \left(\boldsymbol{u}(\boldsymbol{x},t); \partial_t, \partial_{\boldsymbol{x}}\right)$$

The central idea is to set a portion of coefficients c_j to 0, while requiring that $\boldsymbol{f}_a$ and $\boldsymbol{f}$ behave similarly by some predefined measure. While not considered here, additional terms could also be introduced to replace some of the eliminated terms in the original sum, if they are more efficient (from a sparsification perspective) at approximating the physics.

We now apply this general approach within a resolvent analysis framework. If we introduce coefficients c_j within each sub-block of equation 1, we can seek a reduction of this equation by finding a simplified operator $\mathscr{H}_a$ that minimizes the cost function

$$J(\mathbf{c}) = \|\mathscr{H} - \mathscr{H}_a(\mathbf{c})\|_2 + \lambda \|\mathbf{c}\|_1 \tag{5}$$

where $\|\cdot\|_2$ refers to the operator norm, $\mathbf{c} = (c_{11}, c_{21}, c_{22})^T$, and $\mathscr{H}_a$ is given by

$$\mathscr{H}_a = \begin{pmatrix} c_{11}\mathscr{H}_{os} & 0 \\ c_{21} ik_z \mathscr{H}_{sq} U_y \mathscr{H}_{os} & c_{22}\mathscr{H}_{sq} \end{pmatrix} \tag{6}$$

Note that the operator 2-norm has a direct connection with the leading singular value, as $\|\mathscr{H}\|_2 = \sigma_1(\mathscr{H})$. The first term on the right-hand side of equation 5 represents a measure of the difference between the original and sparsified equations, and the second term penalizes the L_1-norm of the coefficient vector $\mathbf{c}$, which promotes a solution where some components of $\mathbf{c}$ are zero. The parameter λ controls the tradeoff between the sparsity of $\mathbf{c}$ and accuracy of the approximation $\mathscr{H}_a$, with a larger λ giving a more sparse approximation. Here the 1-norm is being used rather than the 0-pseudonorm (i.e. penalizing the number of nonzero coefficients) so that the optimization problem is convex, and tractable to be solved using standard convex optimization methods, such as those available in the CVX package (Grant & Boyd, 2014).

RESULTS

Incompressible turbulent channel flow

We first apply the methodology developed in the previous section to incompressible turbulent channel flow, focusing on structures at a specified set of spatio-temporal scales (roughly corresponding to the largest coherent structures expected to arise is such flows). In figure 1 the results of optimizing equation 5 are shown as a function of the sparsification parameter, λ. The left plots show the resulting coefficients (top), as well as the error in the approximation (lower left subplot). We consider two forms of error, the relative error in the estimation of the leading singular value, and the relative error ε given by

$$\varepsilon = \frac{\|\mathscr{H} - \mathscr{H}_a\|_2}{\|\mathscr{H}\|_2} \tag{7}$$

For very small and large λ the approximate operator comes out to be either the original operator or $\mathbf{0}$. However, there

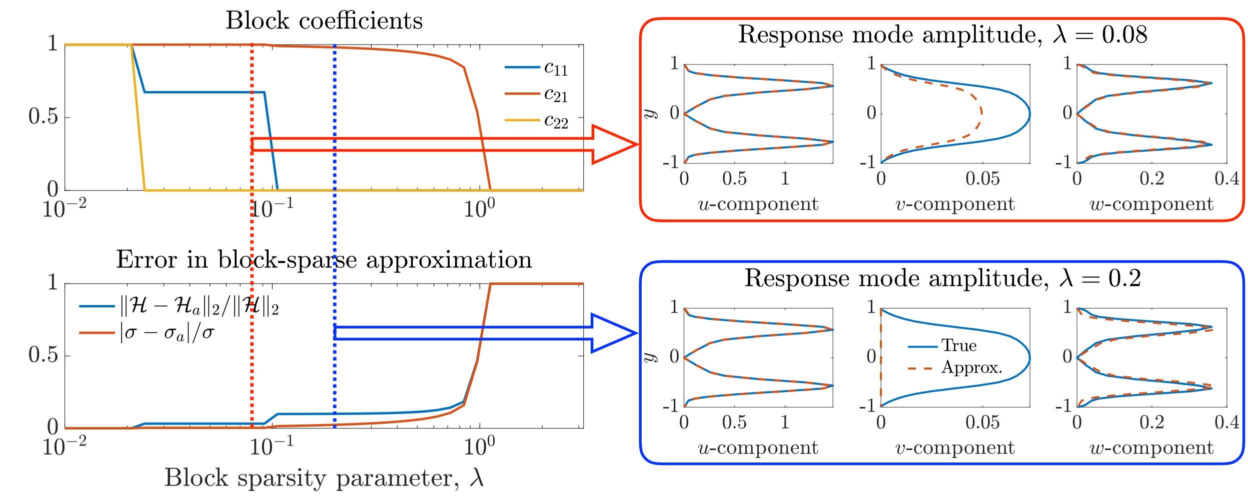

Figure 1: Results obtained from optimizing equation 5 for various values of the sparsification parameter, λ. sparsifying resolvent operator Analysis is for incompressible turbulent channel flow at a friction Reynolds number $Re_\tau = 1000$, streamwise and spanwise wavenumbers $k_x = \frac{\pi}{6}$ and $k_z = \frac{2\pi}{3}$, and a wavespeed (in inner units) $c^+ = \omega/k_x = 20$.

is a region for intermediate λ where one or two of the c_{ij}'s have been set to zero, but where the approximate operator possesses similar properties to the full system. The right plots show a comparison between the amplitude of the velocity components of the leading resolvent response modes for the true and sparsified operators, for two choices of λ, plotted over the wall-normal extent of the domain. For the larger λ, only a single nonzero block is retained. In both cases, we observe that the sparsified operators accurately capture the streamwise (u) and spanwise (w) components of the response, which both relate to the wall-normal vorticity $\hat{\eta} = ik_z\hat{u} - ik_x\hat{w}$. The terms that are truncated are consistent with previous studies, where it has been established that for three-dimensional disturbances of large streamwise extent, the dominant linear amplification mechanism arises to the off-diagonal c_{21} term (Jovanović & Bamieh, 2005; Illingworth, 2020; Jovanović, 2021). This can be explained intuitively by considering the form of equation 1, where the off-diagonal (2,1) block features a composition of two operators. This gives two opportunities for amplification: through $\mathscr{H}_{OS}$ which maps forcing in $\hat{f}_v$ to a response $\hat{v}$, and through $\mathscr{H}_{SQ}$ which here maps this output of $\mathscr{H}_{OS}$ to a response in $\hat{\eta}$.

To test the application of this method over a broader range of scales, we now apply this sparsification method over a broader range of streamwise (k_x) and spanwise (k_z) wavenumbers. Note that for the blockwise 2×2 operator considered in equation 1, there are seven possible sparsification outcomes (excluding the trivial case where all blocks are set to zero), which are enumerated in figure 2(a). In figure 2(b-c), we show the sparsification that is identified for a range of (k_x, k_z) pairs at two different Reynolds numbers, each logarithmically spaced between 10^{-3} and 10^2. For simplicity, we keep the wavespeed fixed at $c^+ = \omega/k_x = 20$, which means that the critical layer (where the mean velocity equals this wavespeed) is also fixed. For the results in figure 2, the sparsification parameter λ is decreased until it first produces a relative error $\varepsilon < 0.1$. We see that there are several distinct regions identified in both cases. In the top left of figures 2(b-c), we tend to identify a mechanism that was also observed in figure 1, when only the off-diagonal block of $\mathscr{H}$ is retained. Conversely, in the lower right of the figures 2(b-c), we instead find that both diagonal blocks are retained, which corresponds to amplification via the independent effects of $\mathscr{H}_{os}$ and $\mathscr{H}_{sq}$. This distinction can be explained in part by the fact that the off-diagonal block is proportional to k_z, so is expected to be most important when $k_z \gg k_x$, and less important for amplification when $k_z \ll k_x$ In between these two regions is a diagonal band when other combinations of these blocks are selected, most notably the case where no blocks are omitted (case 7), indicating that there is no way to eliminate blocks of the original operator while still maintaining a close approximation. At the lower Reynolds number, in addition to this, diagonal band, case 7 is also identified for very large k_z.

To give a sense of the relative importance of the different length scales considered in figure 2(b-c), in figure 2(d-e) we plot the proportion of the total energy captured by the leading two resolvent modes compared to the total energy across all modes at the specified wavenumbers. This quantity, which gives a measure of how close the resolvent is to being a low-rank operator, has been shown to align with the turbulent kinetic energy spectra obtained from direct numerical simulations (Moarref *et al.*, 2013; Bae *et al.*, 2020). Equivalently, regions in these subplots where the contour levels are close to unity indicate that there is a large spectral gap in singular values after the leading two, meaning that one mechanism is dominant (we expect for singular values to often come in pairs, due to the symmetry of channel flow). We observe that the low-rank region approximately coincides with the case 2 region, where only the off-diagonal block of $\mathscr{H}$ is retained in the sparsification procedure. This block maps forcing in wall-normal velocity to response in wall-normal vorticity, via an intermediate response in wall-normal velocity. We see in figure 2 that the streamwise velocity is the largest component of the overall response, and thus also the dominant component of the wall-normal vorticity. This off-diagonal block is thus associated with the lift-up mechanism, where wall-normal velocity fluctuations transfer streamwise momentum towards and away from the wall.

Compressible Couette flow

To explore the broader applicability of the proposed methodology, we now consider laminar compressible Couette flow at a Mach number of 2. This flow has been the subject of several previous studies that utilize a range of linear analysis

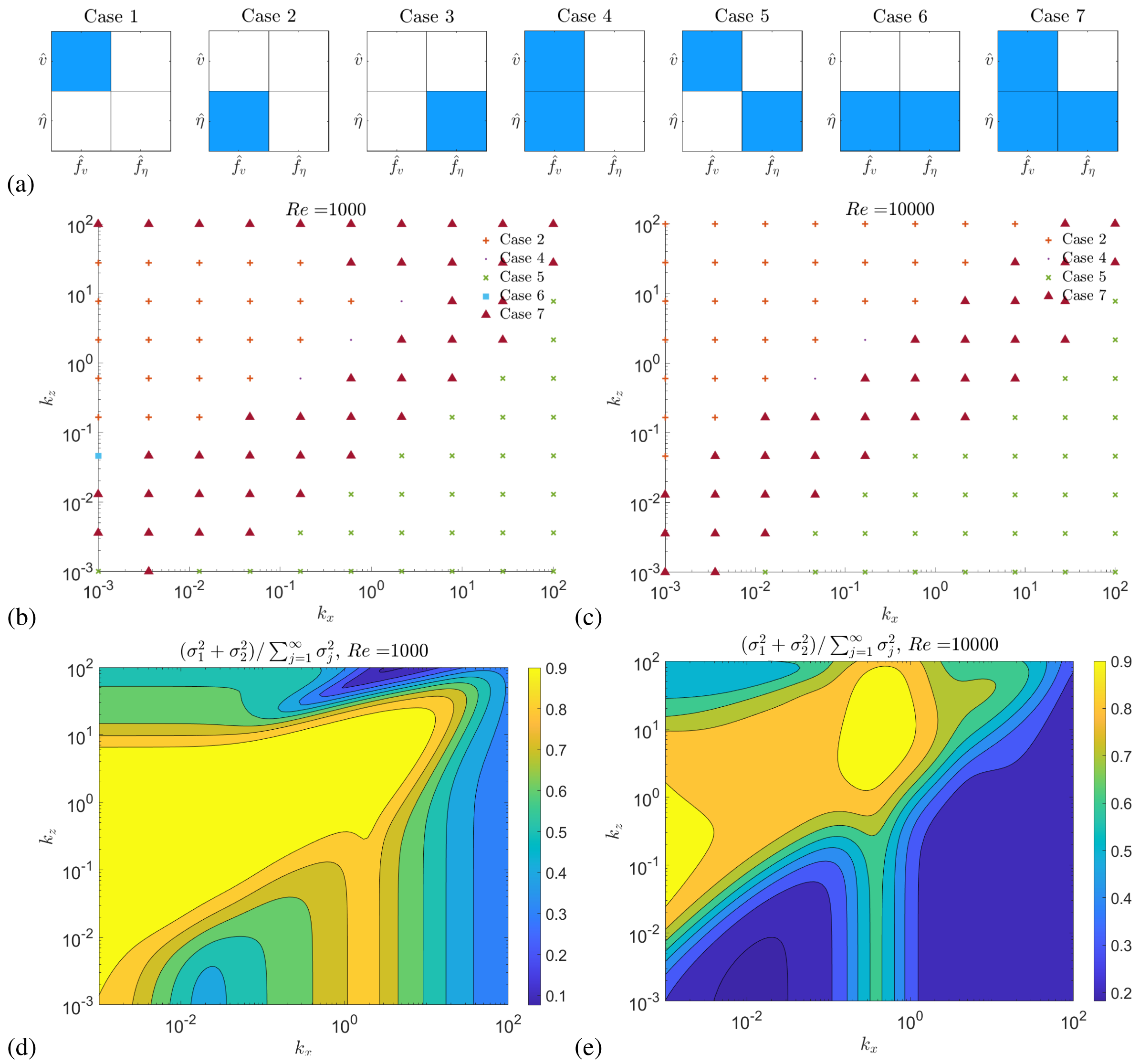

Figure 2: (a) The seven possibilities for simplifying the resolvent operator in wall-normal velocity and vorticity form, where the blue entries denote retained (non-zero) blocks. Subplots (b-c) show the results of sparsifying this operator via equation 5 at friction Reynolds numbers of (b) 1,000 and (c) 10,000 across a range of streamwise (k_x) and spanwise (k_z) wavenumbers. Subplots (d-e) show the extent to which the (full) resolvent operator is low rank for the parameters considered across subplots (b-c)

methods (Duck *et al.*, 1994; Malik *et al.*, 2006; Bhattacharjee *et al.*, 2023), making it a convenient choice for testing our methodology in the compressible regime. While this configuration is laminar, for linearized analyses many findings are qualitatively similar when comparing laminar and turbulent mean profiles. Here, the resolvent operator is formulated in terms of the velocity, density, and temperature, giving a state vector with five components, $\boldsymbol{q} = (u, v, w, \rho, T)$. We use a compressible flow energy norm first formulated by Chu (1965). This means that there are 5×5 blocks in the resolvent operator, substantially increasing the dimensionality of the optimization problem in equation 5. Further details concerning the formulation of the compressible resolvent used can be found in Dawson & McKeon (2019*b*, 2020); Bae *et al.* (2020).

Sample results obtained from applying the proposed methodology are shown in figure 3. This figure shows the form of the optimization problem for the compressible regime in the top left, where we now have the ability to set to zero any of the blocks corresponding to componentwise forcing and response pairs between all of the five state variables. The results of performing the optimization for a range of values of the sparsity parameter λ are shown on the right, with the form of the approximate operator for $\lambda = 0.02$, and the corresponding true and approximate leading resolvent response mode components, shown in the bottom left. As was the case in the incompressible regime, we again find values of λ with small approximation error, but where several of the coefficients c_{ij} have been set to zero. For $\lambda = 0.02$, we observe that a number of the coupling terms between the dynamic (first three components) and thermodynamic (remaining two components) of the resolvent operator are set to zero. In particular, we find zeros in the last two columns of the first three rows of the resolvent operator. This indicates that the response in the velocity components has become independent of forcing in the density and temperature variables. This is consistent, for example, with the Morkovin hypothesis (Morkovin, 1962), which suggests

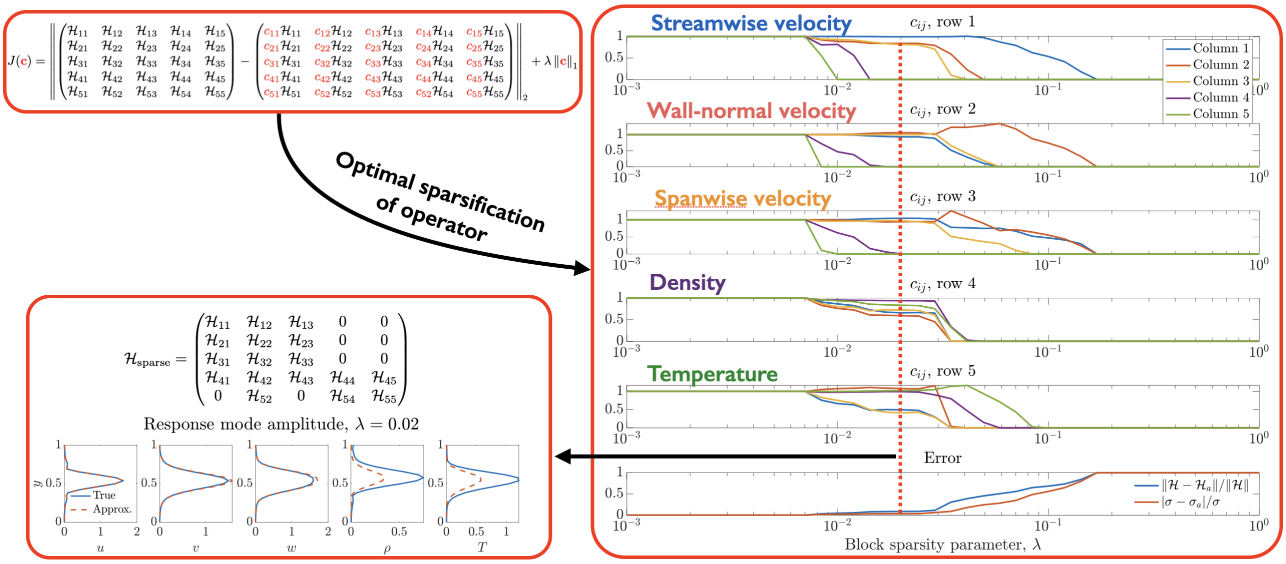

Figure 3: Results from optimizing equation 5 for compressible laminar Couette flow, with $Re = 1000$, $M = 2$, $k_x = k_z = 10$, and $c = 0.5$, showing the elimination of several blocks coupling the dynamic and thermodynamic variables with small error in the approximate operator.

that the dynamics of the velocity field fluctuations are largely the same as those observed in the incompressible regime. This is also consistent with previous findings that the streamwise velocity component of the leading resolvent mode for compressible flow can often be accurately captured from incompressible analyses about the compressible mean field (Dawson & McKeon, 2020). While the density equation (corresponding to the fourth row of $\mathscr{H}$) in the approximation shown in figure 3 retains all terms, the streamwise and spanwise velocity components of the temperature equation are set to zero. The retention of the wall-normal velocity component ($\mathscr{H}_{52}$) can be reasoned by considering the similarity of the dynamics between the temperature and streamwise velocity fields, as consistent with the strong Reynolds analogy (Morkovin, 1962; Smits & Dussauge, 2006). As observed in the previous section, it is typical for large energy amplification to be associated with forcing in wall-normal velocity and response in streamwise velocity. Therefore, if the dynamics of the fluctuating temperature field are similar, then a forcing in wall-normal velocity is also expected to be important for the temperature field, as is identified. For the modes plotted, we find that the velocity components are all accurately captured by the approximate operator, however the thermodynamic variables have their amplitudes reduced in comparison to the true modeLooking at the coefficients c_{ij}, this is likely due to several of them taking nonzero values less than one. While not shown here, it is possible that improved performance could be obtained by setting all nonzero coefficients to take a value of unity, indicating that the non-zero blocks are identical to those of the original operator

CONCLUSIONS

This work has introduced a novel methodology for identifying which terms within a given set of equations are the most important for retaining the properties of the original equations. This provides a framework for simplifying these equations through a sparsification procedure, where terms within the original equation are set to zero. This method was applied in the context of resolvent analysis, to identify simplified operators that possess similar leading singular values and vectors, corresponding to dominant linear energy amplification mechanisms.

For both incompressible and compressible wall-bounded shear flows, the method identified mechanisms that are consistent with mathematical and physical understanding of these systems. For incompressible channel flow, we find that a single block of the governing equations captures the majority of the response across a range of scales for which the resolvent operator is approximately low rank. This block is associated with forcing and response in the wall-normal velocity and vorticity components, respectively, and is associated with the lift-up mechanism. An alternative method to arrive at this conclusion could involve performing componentwise analysis of each block, as performed by Jovanović & Bamieh (2005). For compressible flow, we find (for one set of wavenumbers) a partial decoupling between the velocity components and thermodynamic variables, meaning that the velocity response is largely driven by forcing in the velocity components, rather than via the thermodynamic variables. The response in the density and temperature, however, are coupled to the dynamic variables for the case considered. In particular, we find that the temperature response requires forcing in wall-normal velocity, consistent with its dynamical similarity to the streamwise velocity field via the strong Reynolds analogy.

Here, the sparsification procedure was performed in a blockwise manner. Further work will look to extend this technique such that individual terms within each block can each be isolated and potentially removed. While the physical mechanisms for the flow configurations considered here are already relatively-well understood, further work will apply this automated sparsification methodology to cases where the underlying physics are not as well known. As well as obtaining physical insight, identifying simplified operators can allow for further theoretical analysis, such as the prediction of leading resolvent mode shapes (Dawson & McKeon, 2019*a*, 2020).

ACKNOWLEDGEMENTS

This work is supported by NSF award number CBET-2238770.

REFERENCES

Abreu, L. I., Cavalieri, A. V. G., Schlatter, P., Vinuesa, R. & Henningson, D. S. 2020 Spectral proper orthogonal decomposition and resolvent analysis of near-wall coherent structures in turbulent pipe flows. *Journal of Fluid Mechanics* **900**.

Bae, H. J., Dawson, S. T. M. & McKeon, B. J. 2020 Resolvent-based study of compressibility effects on supersonic turbulent boundary layers. *Journal of Fluid Mechanics* **883**, A29.

Bhattacharjee, D., Mushtaq, T., Seiler, P. J. & Hemati, M. S. 2023 Structured input-output analysis of compressible plane couette flow. In *AIAA SCITECH 2023 Forum*, p. 1984.

Callaham, J. L., Koch, J. V., Brunton, B. W., Kutz, J. N. & Brunton, S. L. 2021 Learning dominant physical processes with data-driven balance models. *Nature Communications* **12** (1), 1–10.

Candès, E. J., Romberg, J. & Tao, T. 2006 Robust uncertainty principles: Exact signal reconstruction from highly incomplete frequency information. *IEEE Transactions on Information Theory* **52** (2), 489–509.

Chu, B.-T. 1965 On the energy transfer to small disturbances in fluid flow (part i). *Acta Mechanica* **1** (3), 215–234.

Dawson, S. T. M. & McKeon, B. J. 2019*a* On the shape of resolvent modes in wall-bounded turbulence. *Journal of Fluid Mechanics* **877**, 682–716.

Dawson, S. T. M. & McKeon, B. J. 2019*b* Studying the effects of compressibility in planar Couette flow using resolvent analysis. In *AIAA Scitech 2019 Forum*, p. 2139.

Dawson, S. T. M. & McKeon, B. J. 2020 Prediction of resolvent mode shapes in supersonic turbulent boundary layers. *International Journal of Heat and Fluid Flow* **85**, 108677.

Duck, P. W., Erlebacher, G. & Hussaini, M. Y. 1994 On the linear stability of compressible plane couette flow. *Journal of Fluid Mechanics* **258**, 131–165.

Foures, D. P. G., Caulfield, C. P. & Schmid, P. J. 2013 Localization of flow structures using-norm optimization. *Journal of Fluid Mechanics* **729**, 672–701.

Grant, M. C. & Boyd, S. P. 2014 CVX: Matlab software for disciplined convex programming, version 2.1.

Hutchins, N. & Marusic, I. 2007 Evidence of very long meandering features in the logarithmic region of turbulent boundary layers. *Journal of Fluid Mechanics* **579**, 1–28.

Hwang, Y. & Cossu, C. 2010 Linear non-normal energy amplification of harmonic and stochastic forcing in the turbulent channel flow. *Journal of Fluid Mechanics* **664**, 51–73.

Illingworth, S. J. 2020 Streamwise-constant large-scale structures in Couette and Poiseuille flows. *Journal of Fluid Mechanics* **889**.

Jovanović, M. R. 2021 From bypass transition to flow control and data-driven turbulence modeling: An input–output viewpoint. *Annual Review of Fluid Mechanics* **53**, 311–345.

Jovanović, M. R. & Bamieh, B. 2005 Componentwise energy amplification in channel flows. *Journal of Fluid Mechanics* **534**, 145–183.

Kline, S. J., Reynolds, W. C., Schraub, F. A. & Runstadler, P. W. 1967 The structure of turbulent boundary layers. *Journal of Fluid Mechanics* **30** (4), 741–773.

Landahl, M. T. 1975 Wave breakdown and turbulence. *SIAM Journal on Applied Mathematics* **28** (4), 735–756.

Loiseau, J.-C. & Brunton, S. L. 2018 Constrained sparse Galerkin regression. *Journal of Fluid Mechanics* **838**, 42–67.

Lopez-Doriga, B., Ballouz, E., Bae, H. J. & Dawson, S. T. M. 2024 Sparse space-time resolvent analysis for statistically-stationary and time-varying flows. *ArXiv preprint arXiv:2404.06331* .

Malik, M., Alam, M. & Dey, J. 2006 Nonmodal energy growth and optimal perturbations in compressible plane Couette flow. *Physics of Fluids* **18** (3), 034103.

McKeon, B. J. & Sharma, A. S. 2010 A critical-layer framework for turbulent pipe flow. *Journal of Fluid Mechanics* **658**, 336–382.

Moarref, R., Sharma, A. S., Tropp, J. A. & McKeon, B. J. 2013 Model-based scaling of the streamwise energy density in high-Reynolds-number turbulent channels. *Journal of Fluid Mechanics* **734**, 275–316.

Morkovin, M. V. 1962 Effects of compressibility on turbulent flows. *Mécanique de la Turbulence* **367**, 380.

Nogueira, P. A. S., Morra, P., Martini, E., Cavalieri, A. V. G. & Henningson, D. S. 2021 Forcing statistics in resolvent analysis: application in minimal turbulent Couette flow. *Journal of Fluid Mechanics* **908**.

Orr, W. M'F. 1907 The stability or instability of the steady motions of a perfect liquid and of a viscous liquid. Part II: A viscous liquid. In *Proceedings of the Royal Irish Academy. Section A: Mathematical and Physical Sciences*, pp. 69–138. JSTOR.

Pickering, E., Rigas, G., Schmidt, O. T., Sipp, D. & Colonius, T. 2021 Optimal eddy viscosity for resolvent-based models of coherent structures in turbulent jets. *Journal of Fluid Mechanics* **917**.

Rosenberg, K. & McKeon, B. J. 2019 Efficient representation of exact coherent states of the Navier–Stokes equations using resolvent analysis. *Fluid Dynamics Research* **51**, 011401.

Rubini, R., Lasagna, D. & Da Ronch, A. 2020 The l1-based sparsification of energy interactions in unsteady lid-driven cavity flow. *Journal of Fluid Mechanics* **905**.

Schmid, P. J. & Henningson, D. S. 2012 *Stability and transition in shear flows*. Springer Science & Business Media.

Skene, C. S., Yeh, C.-A., Schmid, P. J. & Taira, K. 2022 Sparsifying the resolvent forcing mode via gradient-based optimisation. *Journal of Fluid Mechanics* **944**.

Smits, A. J. & Dussauge, J.-P. 2006 *Turbulent shear layers in supersonic flow*. Springer Science & Business Media.

Symon, Sean, Madhusudanan, Anagha, Illingworth, Simon J & Marusic, Ivan 2023 Use of eddy viscosity in resolvent analysis of turbulent channel flow. *Physical Review Fluids* **8** (6), 064601.

Tissot, G., Cavalieri, A. V. G. & Mémin, E. 2021 Stochastic linear modes in a turbulent channel flow. *Journal of Fluid Mechanics* **912**.

Towne, A., Schmidt, O. T. & Colonius, T. 2018 Spectral proper orthogonal decomposition and its relationship to dynamic mode decomposition and resolvent analysis. *Journal of Fluid Mechanics* **847**, 821–867.

Trefethen, L. N., Trefethen, A. E., Reddy, S. C. & Driscoll, T. A. 1993 Hydrodynamic stability without eigenvalues. *Science* **261** (5121), 578–584.

Zhou, J., Adrian, R. J., Balachandar, S. & Kendall, T. M. 1999 Mechanisms for generating coherent packets of hairpin vortices in channel flow. *Journal of Fluid Mechanics* **387**, 353–396.